(14) R. S. Juvet, Jr., V. R. Shaw, and M. A. Khan, *J. Am. Chem. Soc.*, **91**, 3788 (1969).
(15) J. H. von Barner, N. J. Bjerrum, and K. Kiens, *Inorg. Chem.*, **13**, 1708 (1974).
(16) S. N. Flengas and A. Block-Bolten, "Advances in Molten Salt Chemistry", Vol. 2, J. Braunstein, G. Mamantov, and G. P. Smith, Ed., Plenum Press, New York, N.Y., 1973, pp 43, 44.
(17) H. A. Andreasen, N. J. Bjerrum, and C. E. Foverskov, to be submitted for publication.
(18) S. Balt, *Recl. Trav. Chim. Pays-Bas*, **86**, 1025 (1967).

Contribution from the Department of Chemistry, University of Michigan, Ann Arbor, Michigan 48104

Electronic Spectrum of the Tetrachloronickelate(II) Complex at 2.2°K

VAUGHN J. KOESTER[1] and T. M. DUNN*

Received January 7, 1975 AIC500195

The single-crystal electronic spectrum of bis(tetraethylammonium) tetrachloronickelate(II), $(Et_4N)_2NiCl_4$, containing tetragonally distorted $NiCl_4^{2-}$ tetrahedra, was obtained at 2.2°K. Transitions to all the possible crystal field terms arising from the configuration d^8 were identified with the exception of the transition terminating on the ^1A level arising from the free-ion ^1S term. In the strongly absorbing red region, the polarized single-crystal spectrum of Cs_3ZnCl_5 doped with Ni^{2+} was also obtained. Electronic transitions are assigned on the basis of a semiempirical calculation performed within the framework of the crystal field model for tetrahedral coordination. Effects on the spectrum due to spin–orbit coupling and tetragonal distortion are analyzed and discussed. The large splitting in the $^3T_1(^3P)$ manifold is assigned as being due to these combined effects. The emission spectrum of $(Et_4N)_2ZnCl_4$ doped with Ni^{2+} was obtained at 2.2°K. A progression in an Et_4N^+ fundamental, based on $NiCl_4^{2-}$ electronic and vibronic origins, is taken as evidence for significant anion to cation coupling in the crystal.

Introduction

The electronic absorption spectra of tetrahedral complexes of Ni^{2+} have been studied extensively.[2-15] The most detailed analyses were performed on spectra of single-crystal (host) materials doped with nickel and cooled to approximately 4°K.[8,10,12,15] In the earlier investigations, using oxide and sulfide hosts,[8,10,12] the presence of complicated phonon structure prevented a detailed analysis of the spectra. Host materials which contain discrete tetrahedral moieties can be used to minimize this difficulty and recently the polarized absorption spectrum of the $NiCl_4^{2-}$ species in a Cs_3MgCl_5 host was obtained.[15]

The strongest band system in the red region has been assigned in all cases to the $^3T_1(^3P) \leftarrow {}^3T_1(^3F)$ transition on the basis of semiempirical crystal field calculations. Effects due to spin–orbit coupling and lower symmetry fields were also considered, particularly by Couch and Smith.[15]

Since, in previous investigations, spectra were obtained with relatively dilute crystals, only the strongest transitions have been characterized. For this reason, we have obtained the absorption spectrum of the $NiCl_4^{2-}$ complex using the pure $(Et_4N)_2NiCl_4$ compound which allows observation of several very weak electronic transitions.

The crystal field energy level pattern for tetrahedral Ni^{2+} (d^8) was calculated by Liehr and Ballhausen[16] (abbreviated LB). Their calculation parameterized the spin–orbit coupling in terms of the term constant λ and expressed the electron repulsion in terms of the Slater–Condon–Shortley F_2 and F_4 parameters. The parameter values used by LB were $\lambda = -275$ cm^{-1}, $F_2 = 14F_4$, and $F_4 = 90$ cm^{-1} and a similar diagram is shown in Figure 1. This diagram shows the ground state, derived from the $^3T_1(^3F)$ state, to be Γ_1, and separated from the next lowest level by a large enough energy so that, at 4°K, only Γ_1 is occupied. In T_d symmetry the transition $\Gamma_5 \leftarrow \Gamma_1$ is allowed (T_d notation). In the compounds being investigated the site symmetry of the $NiCl_4^{2-}$ complex is D_{2d}, so that $\Gamma_1 \rightarrow A_1$ and $\Gamma_5 \rightarrow E + B_2$; i.e., we have the electric dipole selection rules $E \leftarrow A_1$ and $B_2 \leftarrow A_1$. Calculations of the LB type were used in making a preliminary assignment of the spectrum.

In T_d symmetry there are four fundamental vibrations of the $NiCl_4^{2-}$ moiety. These are designated as $\nu_1(a_1)$, $\nu_2(e)$, $\nu_3(t_2)$, and $\nu_4(t_2)$. Infrared spectra give the $\nu_3(t_2)$ and $\nu_4(t_2)$ fundamentals at 289 and 112 cm^{-1}, respectively.[17,18] From the $ZnCl_4^{2-}$ Raman spectrum[19] in the compound $(Et_4N)_2ZnCl_4$, the $\nu_1(a_1)$ and $\nu_2(e)$ frequencies are determined to be 280 and 60 cm^{-1}, respectively. It is expected that the $NiCl_4^{2-}$ $\nu_1(a_1)$ and $\nu_2(e)$ fundamentals are approximately equal to these values. Indeed the $\nu_2(e)$ fundamental was tentatively assigned at 79 cm^{-1}.[18] In D_{2d} we designate a vibration according to the T_d fundamental from which it is derived; e.g., $\nu_2(e)$ gives rise to $a_1(\nu_2)$ and $b_1(\nu_2)$.

Experimental Section

1. $(Et_4N)_2NiCl_4$ and $(Et_4N)_2ZnCl_4$. Since the preparations of the zinc and nickel compounds are identical, only the nickel compound will be discussed. These compounds were previously characterized by Gill and Nyholm[4] and their methods were followed precisely.

A solution of the complex in absolute EtOH was slowly evaporated in a desiccator containing concentrated H_2SO_4, and single crystals suitable for spectroscopic analysis were obtained. The crystals were stored in a desiccator or under Nujol because of their deliquescent nature.

The crystal system to which $(Et_4N)_2NiCl_4$ belongs is tetragonal.[20] Its space group is $P4_2/nmc$ (D_{4h}^{15}) with two formula units per unit cell. This compound has been shown to be isomorphous with the $(Et_4N)_2ZnCl_4$ salt.[17,21] In both cases the MCl_4^{2-} species exist as discrete molecular units with a site symmetry at each nickel position of D_{2d}. The molecule is situated such that the c crystallographic axis bisects the smaller Cl–Ni–Cl angle and coincides with the z cartesian axis of the D_{2d} point group. In addition, the x and y cartesian axes of the D_{2d} point group are rotated by 45° with respect to the a and b crystallographic axes.

The structure also appears to be disordered in such a way that the exact nuclear geometry of the $NiCl_4^{2-}$ species is uncertain. Any distortion from D_{2d} symmetry, however, is apparently very small and, on the average, D_{2d} symmetry is maintained at the nickel sites.

2. $(Et_4N)_2Zn(Ni)Cl_4$. Sufficient quantities of $(Et_4N)_2NiCl_4$ and $(Et_4N)_2ZnCl_4$ were added to absolute alcohol to saturate the solution at its boiling point. The solution was filtered and the EtOH was added to the filtrate to dissolve the precipitate which formed. Slow evaporation yielded very small light blue single crystals. The nickel concentration was not precisely determined. Since the crystal size

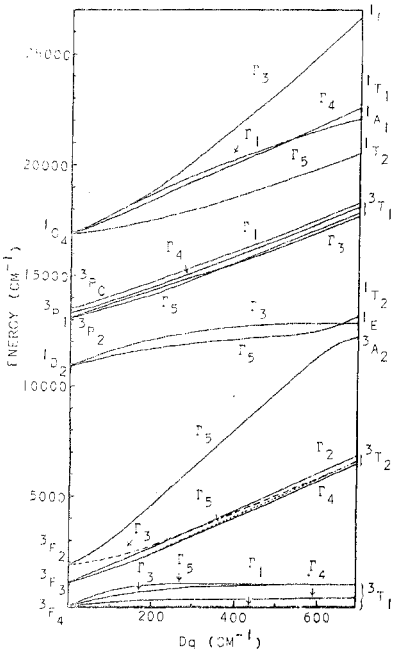

Figure 1. Energy level diagram for the Ni^{2+}, $[Ar]3d^8$, electron configuration in a tetrahedral crystal field with $\lambda = -275$ cm^{-1}, $F_4 = 90$ cm^{-1}, and $F_2 = 14F_4$. Energy is expressed relative to the $\Gamma_1(^3F_4)$ ground state. The free-ion term symbols appear on the left, whereas the crystal field state designations are on the right. The $^1A_1$ ($^1S_0$) state is at very high energy and is not included.

was not suitable for absorption experiments, only emission experiments were performed with the crystals obtained in this way.

3. $Cs_3Zn(Ni)Cl_5$. Due to the possible formation and presence of zinc oxychlorides in $ZnCl_2$, it was distilled in vacuo in a Vycor apparatus. Provision was made to add to this a stoichiometric amount of dried CsCl mixed with anhydrous $NiCl_2$. The nickel concentration in the doped Cs_3ZnCl_5 was 0.5%. In order to obtain a measured amount of $ZnCl_2$, its density at the melting point was determined to be 2.54 ± 0.08 g/cm^3.

The sample was zone refined by approximately 15 passes through a refining furnace. A suitable portion of the sample was added to a tapered Vycor tube and sealed in vacuo (no exposure to atmospheric water vapor occurred prior to this transfer). The crystal used in the experiments was grown by the Bridgman technique. Since single crystals of Cs_3ZnCl_5, grown by this technique, were characterized by van Stapele et al.,[22] no further characterization was considered necessary.

The compound Cs_3ZnCl_5 is isomorphous with the $CsCoCl_5$ compound,[25] which is tetragonal.[23,24] The space group is $14/mcm$ (D_{4h}^{18}) with four formula units per unit cell. Each dipositive cobalt ion is surrounded by four chloride ions in such a way that the $CoCl_4^{2-}$ species can be considered as a discrete molecular entity. The site symmetry at each cobalt position is D_{2d} and the $CoCl_4^{2-}$ moiety is oriented such that the c crystallographic axis bisects the smaller Cl–Co–Cl angle.

4. Apparatus. Spectra in the region 4000 cm^{-1} (25,000 Å) to approximately 20,000 cm^{-1} (5000 Å) were obtained using a Cary Model 14 spectrophotometer. Only the region up to approximately 13,500 cm^{-1} was studied in detail with this apparatus. All spectra were taken with the slit control and the gain was adjusted to obtain a reasonable signal-to-noise ratio.

Spectra from approximately 13,500 cm^{-1} (7000 Å) to 25,000 cm^{-1} (4000 Å) were obtained in the first order of a 1.5-m Bausch and Lomb grating spectrograph. Emission spectra were obtained using a 1000-W Osram high-pressure mercury–xenon lamp. Wavelength calibration was obtained from an iron arc emission spectrum. A Joyce–Loebl microdensitometer was used to record the photographic images.

Samples were cooled to 2.2°K in a total immersion dewar and polarization measurements were performed using a Polacoat fused-silica laminated polarizer. The dewar used in this work was designed and built in our Chemistry Department. It is of stainless steel and brass external construction with a glass and fused-silica insert.

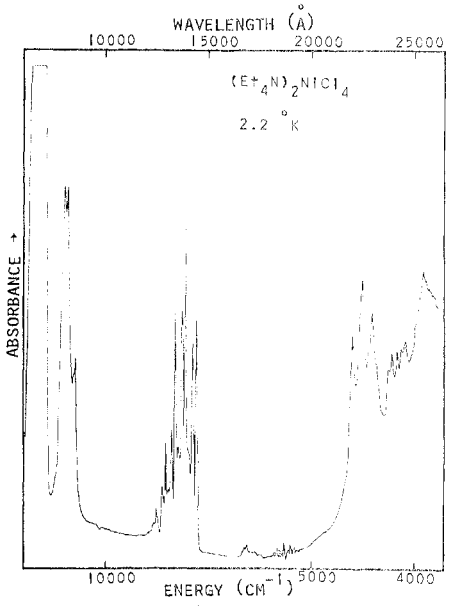

Figure 2. Near-infrared–visible single-crystal spectrum of $(Et_4N)_2NiCl_4$ at 2.2°K (26,000–6000 Å).

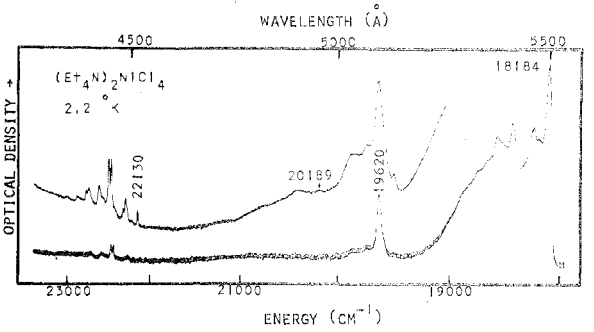

Figure 3. Single-crystal spectrum of $(Et_4N)_2NiCl_4$ at 2.2°K in the visible region (5600–4250 Å).

The fused-silica part of the insert is of square-section high optical quality fused silica of 2-cm side and internal windows are, therefore, unnecessary. All spectra were taken under conditions of total immersion of the sample and the helium was pumped to reduce the temperature to the λ point. Temperatures were measured by measuring the pressure of gaseous helium in equilibrium with the "liquid".

Results

1. Absorption Spectra. Figure 2 presents the 2.2°K spectrum of $(Et_4N)_2NiCl_4$ in the near-infrared–visible region. If the very strong (truncated) band centered at 6800 Å (14,700 cm^{-1}) is assigned to the $^3T_1(^3P) \leftarrow {}^3T_1(^3F)$ transition and if $Dq \approx 500$ cm^{-1}, Figure 1 shows that the band systems to lower energy can be assigned as transitions to the states $^1T_2(^1D)$, $^1E(^1D)$, $^3A_2(^3F)$ and $^3T_2(^3F)$. The $^1T_2(^1D)$, $^1E(^1D)$ pair is centered at 12,100 cm^{-1} (8280 Å), $^3A_2(^3F)$ is at 7270 cm^{-1} (13,750 Å), and $^3T_2(^3F)$ extends from about 26,000 to 21,000 Å. The features appearing at 5930 cm^{-1} (6860 Å) in Figure 1 are combination and overtone bands arising from C–H stretching fundamentals in the $(C_2H_5)_4N^+$ cation. The oscillatory feature immediately to lower energy is instrumental in origin.

The region between about 15,000 and 18,000 cm^{-1} shows no detectable absorption systems and Figure 3 represents the spectrum obtained in the visible region from 18,200 cm^{-1} (5500 Å) to 23,500 cm^{-1} (4250 Å). According to the LB calculation,[16] in the range $Dq < 500$ cm^{-1}, these transitions are to the $^1T_2$, $^1T_1$, $^1A_1$, and ^1E states, derived from the ^1G term. Based on the calculated order, $^1T_2 < {}^1T_1 < {}^1A_1 < {}^1E$, the

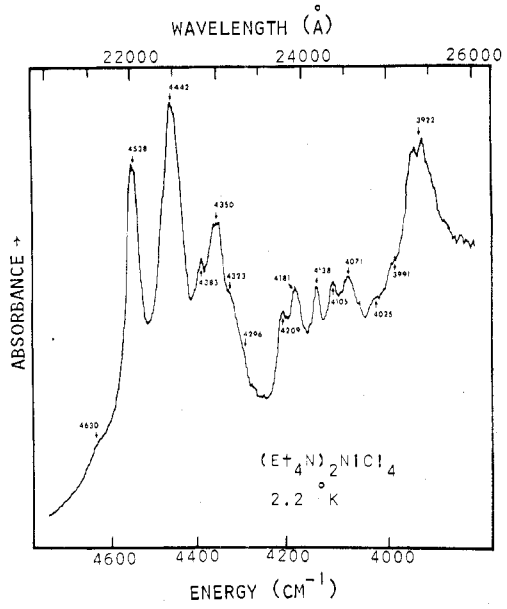

Figure 4. $^3T_2(^3F) \leftarrow {}^3T_1(^3F)$ transition in the single-crystal spectrum of $(Et_4N)_2NiCl_4$ at 2.2°K (26,000–21,000 Å).

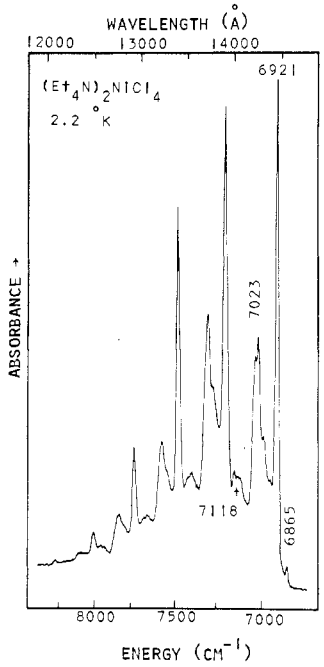

Figure 5. $^3A_2(^3F) \leftarrow {}^3T_1(^3F)$ transition in the single-crystal spectrum of $(Et_4N)_2NiCl_4$ at 2.2°K (14,500–12,000 Å).

bands in this spectrum can be assigned. Thus, we have transitions to the $^1T_2(^1G)$ state in the range 18,200 cm^{-1} (5500 Å) to 19,200 cm^{-1} (5200 Å), to the $^1T_1(^1G)$ and $^1A_1(^1G)$ states in the range 19,500 cm^{-1} (5200 Å) to 21,000 cm^{-1} (4700 Å), and to the $^1E(^1G)$ state in the range 22,000 (4500 Å) to 23,000 cm^{-1} (4300 Å). These transitions will be analyzed individually below.

$^3T_2(^3F) \leftarrow {}^3T_1(^3F)$. Figure 4 gives the spectrum obtained in the region 26,000–21,000 Å. The inclusion of spin–orbit coupling splits the $^3T_2(^3F)$ crystal field level into four states, viz., Γ_2, Γ_3, Γ_4, and Γ_5. In *Td* symmetry, one purely electronic transition ($\Gamma_5 \leftarrow \Gamma_1$) and five vibronic origins are allowed, based on all states except Γ_2. Since no vibrational progressions are seen in this spectrum, it is impossible to locate the origins.

The overall width of the system is ~700 cm^{-1}. This is close to the overall 400-cm^{-1} splitting estimated from the LB calculation, suggesting that there is no absorption outside this region due to the $^3T_2(^3F)$ state. In view of the lack of extended structure, unambiguous assignments are not possible for this system. The location (in cm^{-1}) of each band and shoulder, consistently reproduced in many experiments, is given in the figure.

$^3A_2(^3F) \leftarrow {}^3T_1(^3F)$. This transition has been previously studied in $(Et_4N)_2NiCl_4$ and $(Et_4N)_2NiBr_4$ by Mooney, Nuttall, and Smith,[27] who claimed to have done their experiment at 5°K. It is clear from the spectra presented here (which do not differ significantly from those we obtained at 4.2°K) that their samples were at a considerably higher temperature than their sample block. The much higher resolution obtained in the present work enables a much more definitive vibrational analysis although, of course, both groups agree upon the identification of the electronic species.

Figure 5 presents the spectrum of the $^3A_2(^3F) \leftarrow {}^3T_1(^3F)$ transition. With inclusion of spin–orbit coupling, the $^3A_2$ state becomes Γ_5 and in *D2d* symmetry the states E and B_2 are obtained. Since the transitions $B_2 \leftarrow A_1$ and $E \leftarrow A_1$ are allowed, the bands at 6865 and 6921 cm^{-1} are assigned as these origins. Based on each origin is a progression in five quanta of the $a_1(\nu_1)$ totally symmetric fundamental, with a frequency of 270 cm^{-1}.

The remaining bands at 6954, 6988, 7023, (the mean of the 7017 and 7030 cm^{-1}), and 7118 cm^{-1} are vibronic origins. The $a_1(\nu_1)$ progression can also be seen based on the stronger vibronic origins.

Since the 96- and 109-cm^{-1} intervals between the 6921-cm^{-1} origin and the 7017- and 7030-cm^{-1} bands, respectively, correspond closely to the ground-state $\nu_4(t_2)$ fundamental,[19] they are assigned as arising from the $b_2(\nu_4)$ and $e(\nu_4)$ vibrational components in *D2d*. From group-theoretical considerations, vibronic origins due to both of these fundamentals are allowed only if the 6921-cm^{-1} origin is assigned to the $E(\Gamma_5)$ component. Similarly the relatively broad 7118-cm^{-1} band appears to arise from the second quantum and combination of these vibrations. The 67-cm^{-1} interval between the 6921-cm^{-1} origin and the 6988-cm^{-1} band corresponds to the unresolved components of the $\nu_2(e)$ fundamental.

The selection rules allow only the $e(\nu_4)$ component, based on the $B_2(\Gamma_5)$ origin, to appear and this accounts for the 6954-cm^{-1} band, with its 89-cm^{-1} separation from the 6865-cm^{-1} origin. Since the same splittings are expected for this vibration based on the $E(\Gamma_5)$ origin, the 7017- and 7030-cm^{-1} bands can be assigned to the $e(\nu_4)$ and $b_2(\nu_4)$ vibrations, respectively. The complete analysis of this spectrum is presented in Table I. The different intensities of the two electronic origins are due to a combination of the (unknown) sample orientation, required by the crystal growth habit, coupled with their intrinsic intensity differences.

Assuming the $\Gamma_5 \leftarrow \Gamma_1$ origin as 6900 cm^{-1} gives $Dq \approx 350$ cm^{-1}.

$^1T_2(^1D) \leftarrow {}^3T_1(^3F)$ and $^1E(^1D) \leftarrow {}^3T_1(^3F)$. Some spectra of the various systems arising from the ^1G term of Ni^{2+} in the tetraethylammonium chloride and bromide have been previously reported by Mooney, Nuttall, and Smith[28] and much the same comments apply to this work as that of their study of the $^3A_2 \leftarrow {}^3T_1(^3F)$ system at 7400 cm^{-1}. We believe that our spectra are sufficiently better resolved for us to prefer our vibrational analysis but again, both groups agree on the gross electronic identifications.

Having no net electron spin, $^1T_2$ and ^1E become Γ_5 and Γ_3, respectively. The calculation by LB shows the energy order $\Gamma_5 < \Gamma_3$ for all $Dq = 1400$ cm^{-1} so that the 11,694-cm^{-1} band in Figure 6 is assigned as the allowed $\Gamma_5 \leftarrow \Gamma_1$ origin. This band appears in the 77°K spectrum (not shown) at about 11,700 cm^{-1}. A band also appears in the 77°K spectrum at about 12,900 cm^{-1} and is assigned to the $\Gamma_3 \leftarrow \Gamma_1$ transition.

The only other transition which can be assigned with

Table I. Analysis of the $^3A_2(^3F) \leftarrow {}^3T_1(^3F)$ Transition in the Compound $(Et_4N)_2NiCl_4$[a]

Origin, cm^{-1}	Band energy, cm^{-1}	Energy diff, cm^{-1}	Assignment
Electronic: 6865			$B_2(\Gamma_5)$
	6954	89	$B_2(\Gamma_5) + e(\nu_3)$
	7143	278	$B_2(\Gamma_5) + a_1(\nu_1)$
Electronic: 6921			$E(\Gamma_5)$
	6988	67	$E(\Gamma_5) + a_1(\nu_2)$ $E(\Gamma_5) + b_1(\nu_2)$
	7017	96	$E(\Gamma_5) + e(\nu_3)$
	7030	109	$E(\Gamma_5) + b_2(\nu_3)$
	7118	197	$E(\Gamma_5) + 2e(\nu_3)$ $E(\Gamma_5) + e(\nu_3) + b_2(\nu_3)$ $E(\Gamma_5) + 2b_2(\nu_3)$
	7194	273	$E(\Gamma_5) + a_1(\nu_1)$
	7468	547	$E(\Gamma_5) + 2a_1(\nu_1)$
	7738	817	$E(\Gamma_5) + 3a_1(\nu_1)$
	8006	1085	$E(\Gamma_5) + 4a_1(\nu_1)$
	8273	1352	$E(\Gamma_5) + 5a_1(\nu_1)$
Vibronic: 6988			^{ev}E
	7262	274	$^{ev}E + a_1(\nu_1)$
	7536	548	$^{ev}E + 2a_1(\nu_1)$
	7800	812	$^{ev}E + 3a_1(\nu_1)$
Vibronic: 7023[b]			$^{ev}B_2$ ^{ev}E
	7289	266	$^{ev}B_2 + a_1(\nu_1)$ $^{ev}E + a_1(\nu_1)$
	7565	542	$^{ev}B_2 + 2a_1(\nu_1)$ $^{ev}E + 2a_1(\nu_1)$
	7834	811	$^{ev}B_2 + 3a_1(\nu_1)$ $^{ev}E + 3a_1(\nu_1)$
Vibronic: 7118			$^{ev}B_2$ ^{ev}E
	7386	268	$^{ev}B_2 + a_1(\nu_1)$ $^{ev}E + a_1(\nu_1)$
	7654	536	$^{ev}B_2 + 2a_1(\nu_1)$ $^{ev}E + 2a_1(\nu_1)$
	7935	817	$^{ev}B_2 + 3a_1(\nu_1)$ $^{ev}E + 3a_1(\nu_1)$

[a] The associated spectrum appears in Figure 5. [b] This value represents the mean of the 7017- and 7030-cm^{-1} bands.

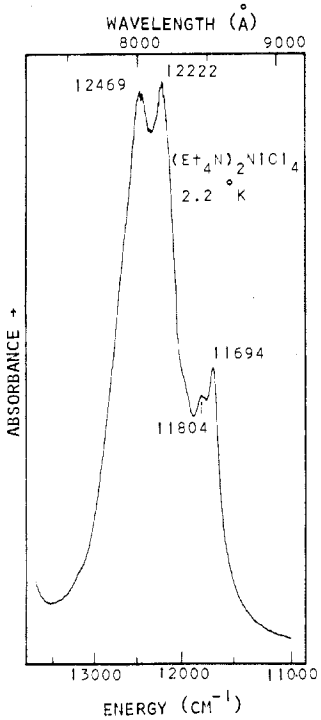

Figure 6. $^1T_2(^1D) \leftarrow {}^3T_1(^3F)$ and $^1E(^1D) \leftarrow {}^3T_1(^3F)$ transitions in the single-crystal spectrum of $(Et_4N)_2NiCl_4$ at 2.2°K (9000–7500 Å).

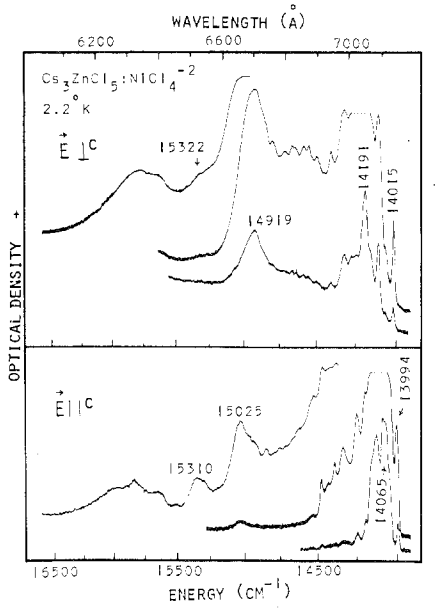

Figure 7. Polarized single-crystal spectrum of $Cs_3Zn(Ni)Cl_5$ at 2.2°K, showing the $^3T_1(^3T_1(^3F)$ transition (7200–6000 Å). The three tracings for each spectrum represent different exposure times.

confidence is at 11,804 cm^{-1}. This band is due to the $\nu_4(t_2)$ fundamental since it is displaced by 110 cm^{-1} from the 11,694-cm^{-1} origin. The remaining unresolved structure is vibronic structure associated with both the Γ_5 and Γ_3 states.

The maximum in the 77°K spectrum at 12,900 cm^{-1} is shifted to lower energy in the 2.2°K spectrum for two reasons. The most obvious reason is the difference in the Boltzmann distribution at these two temperatures. The other is that at 77°K this band is on the side of the extremely intense $^3T_1(^3P) \leftarrow {}^3T_1(^3F)$ transition. The result is that the observed maximum of the weaker transition will be shifted towards the very strong transition (i.e., to higher energy). The actual band maximum therefore occurs at a lower energy than observed. Thus, the 12,469-cm^{-1} band in the 2.2°K spectrum is probably the vibronic maximum for the $\Gamma_3 \leftarrow \Gamma_1$ transition. The 12,222-cm^{-1} band is similarly associated with the $\Gamma_5 \leftarrow \Gamma_1$ transition.

$^3T_1(^3P) \leftarrow {}^3T_1(^3F)$. As mentioned previously, the very intense absorption extending from 14,000 cm^{-1} (7250 Å) to 16,500 cm^{-1} (6250 Å) was assigned to the $^3T_1(^3P) \leftarrow {}^3T_1(^3F)$ transition. The polarized spectrum of the doped $Cs_3Zn(Ni)Cl_5$ compound is given in Figure 7. It is assumed that the $NiCl_4^{2-}$ moieties in the doped crystal have the same geometry (D_{2d}) and the same orientation as those of the equivalent $ZnCl_4^{2-}$ hosts. The three curves in the top and bottom of this spectrum correspond to different exposure times. It is to be noted that only two bands are clearly coincident in both polarizations. These bands, at 14,065 and 14,191 cm^{-1}, result from slightly incomplete polarizations. Also, it is estimated that intensity maxima in the $E \perp c$ spectrum are approximately 5 times greater than in the $E \| c$ spectrum.

With spin–orbit coupling the $^3T_1$ level becomes Γ_1, Γ_3, Γ_4, and Γ_5. The LB calculation at $Dq \approx 350$ cm^{-1} shows the ordering of states as $\Gamma_5 < \Gamma_3 < \Gamma_4 < \Gamma_1$. The completely polarized transitions at 13,944 cm^{-1} and 14,015 cm^{-1} are therefore assigned as the $B_2(\Gamma_5) \leftarrow A_1(\Gamma_1)$ and $E(\Gamma_5) \leftarrow A_1(\Gamma_1)$ origins, respectively. No extended progression in the $a_1(\nu_1)$ vibration is observed, based on either of these origins.

By far the strongest band in the $E \perp c$ spectrum occurs at 14,191 cm^{-1}. It does not represent a vibronic origin based on the $B_2(\Gamma_5)$ and $E(\Gamma_5)$ states since it is separated from them by 176 and 197 cm^{-1}, respectively. Neither is it a member

Table II. Analysis of the $^3T_1(^3P) \leftarrow {}^3T_1(^3F)$ Transition in the Compound $Cs_3Zn(Ni)Cl_5$[a]

Origin, cm^{-1}	Band energy, cm^{-1}	Energy diff, cm^{-1}	Assignment	Polarizn
Electronic: 14,015			$E(\Gamma_5)$	$\perp$
			$E(\Gamma_5) + a_1(\nu_2)$	$\perp$
	Unobsd		$E(\Gamma_5) + b_1(\nu_2)$	$\perp$
	14,107	92	$E(\Gamma_5) + b_2(\nu_4)$	$\perp$
	14,119	104	$E(\Gamma_5) + e(\nu_4)$	$\parallel$
	14,319	304	$E(\Gamma_5) + b_2(\nu_3)$	$\perp$
	14,328	314	$E(\Gamma_5) + e(\nu_3)$	$\parallel$
Electronic: 13,994			$B_2(\Gamma_5)$	$\parallel$
	14,079	85	$B_2(\Gamma_5) + a_1(\nu_2)$	$\parallel$
	Unobsd		$B_2(\Gamma_5) + e(\nu_4)$	$\perp$
	14,308	314	$B_2(\Gamma_5) + e(\nu_3)$	$\perp$

[a] The associated spectrum appears in Figure 7.

Table III. Analysis of the $^1T_2(^1G) \leftarrow {}^3T_1(^3F)$ Transition in the Compound $(Et_4N)_2NiCl_4$[a]

Origin, cm^{-1}	Band energy, cm^{-1}	Energy diff, cm^{-1}	Assignment
Electronic: 18,184			Γ_5
	18,270	86	$\Gamma_5 + \nu_2(e)$
	18,310	126	$\Gamma_5 + \nu_4(t_2)$
	18,471	287	$\Gamma_5 + \nu_1(a_1)$
	18,755	571	$\Gamma_5 + 2\nu_1(a_1)$
Vibronic: 18,270			$^{ev}\Gamma_5$
	18,561	291	$^{ev}\Gamma_5 + \nu_1(a_1)$
Vibronic: 18,310			$^{ev}\Gamma_5$
	18,594	284	$^{ev}\Gamma_5 + \nu_1(a_1)$

[a] The associated spectrum appears in Figure 8.

of a progression associated with these origins, since no additional member can be seen to higher energy. It is therefore reasonable to assign it as a vibronic origin, due to the e component of the $\nu_3(t_2)$ or $\nu_4(t_2)$ fundamental, based on the $A_1(\Gamma_3)$ or $B_1(\Gamma_3)$ origins, since it is completely (x, y) polarized. The $A_1(\Gamma_3)$ and $B_1(\Gamma_3)$ origins cannot be distinguished in these polarized spectra since sufficiently detailed vibronic structure is not present. A summary of additional assignments is presented in Table II. Also, many of the remaining features up to $\sim$14,850 cm^{-1} can be assigned assuming a lattice vibration of $\sim$50 cm^{-1}.

Since the transition $E \leftarrow A_1$ is allowed in D_{2d} and since the Γ_4 state is expected to lie at higher energy than Γ_5 or Γ_3, the very strong and rather diffuse feature centered at 14,919 cm^{-1} in the $E \perp c$ spectrum is assigned to the $E(\Gamma_4)$ component of the Γ_4 state. The band at 15,025 cm^{-1} in the $E \parallel c$ spectrum is approximately an order of magnitude weaker by comparison and corresponds to vibronic structure based on the transitions to both the E and A_2 components of Γ_4. The shoulder at 14,917 cm^{-1} probably corresponds to incomplete polarization.

The origin of this $E \leftarrow A_1$ transition cannot be located due to the diffuseness of the spectrum. The band at 15,310 cm^{-1} in the $E \parallel c$ spectrum (or the shoulder at 15,322 cm^{-1} in the $E \perp c$ spectrum), however, is probably additional vibronic structure based on the E and A_2 components of Γ_4. It has a very similar appearance to the diffuse band at 15,025 cm^{-1} and is separated from it by $\sim$300 cm^{-1}.

The diffuse bands in the range 15,600–16,000 cm^{-1} are assigned as vibronic transitions based on the Γ_1 origin.

The unpolarized $(Et_4N)_2NiCl_4$ spectrum (not shown) is very similar in all respects to the z-polarized spectrum in Figure 7. This is probably due to the comparatively higher extinction in the (x, y) polarization.

$^1T_2(^1G) \leftarrow {}^3T_1(^3F)$. In the singlet system, $^1T_2$ becomes Γ_5. Since the electronic transition $\Gamma_5 \leftarrow \Gamma_1$ is allowed and since the Γ_5 state is calculated to be at the lowest energy of the states derived from the ^1G term, the very strong feature at 18,184 cm^{-1} in Figure 8 is assigned as this origin. Associated with this origin is a considerable amount of vibronic structure which becomes more and more diffuse to higher energy. Clearly discernible, however, are two quanta of the totally symmetric $\nu_1(a_1)$ fundamental, having a frequency of 287 cm^{-1}, which account for the bands at 18,471 and 18,755 cm^{-1}. The complete analysis is presented in Table III. Sufficient structure is not present to analyze the effects of the tetragonal distortion.

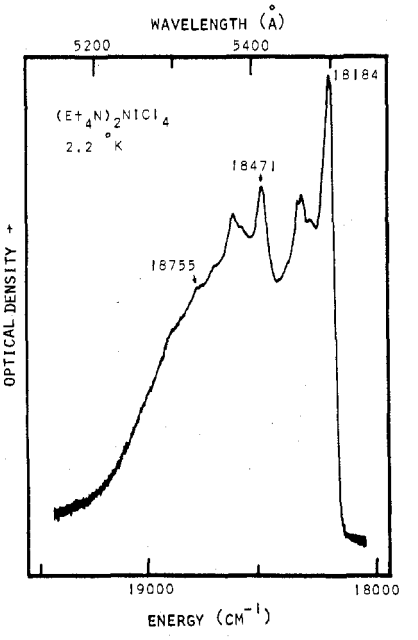

Figure 8. $^1T_2(^1G) \leftarrow {}^3T_1(^3F)$ transition in the single-crystal spectrum of $(Et_4N)_2NiCl_4$ at 2.2°K (5600–5100 Å).

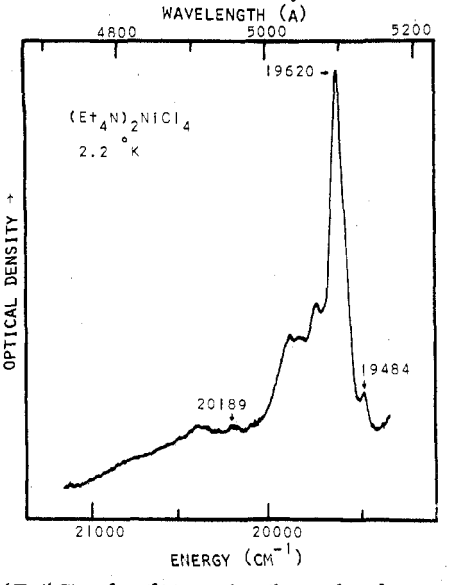

Figure 9. $^1T_1(^1G) \leftarrow {}^3T_1(^3F)$ and $^1A_1(^1G) \leftarrow {}^3T_1(^3F)$ transitions in the single-crystal spectrum of $(Et_4N)_2NiCl_4$ at 2.2°K (5200–4700 Å).

$^1T_1(^1G) \leftarrow {}^3T_1(^3F)$ and $^1A_1(^1G) \leftarrow {}^3T_1(^3F)$. The relatively strong maximum at 19,620 cm^{-1} in Figure 9 is associated with the $^1T_1(^1G) \leftarrow {}^3T_1(^3F)$ transition. In the singlet system, $^1T_1$ becomes Γ_4 and $^1A_1$ becomes Γ_1. Even though the transition to Γ_4 is forbidden, the transition to the $E(\Gamma_4)$ component is allowed in D_{2d}. Therefore the 19,484-cm^{-1} band is assigned as being the $E(\Gamma_4)$ origin.

Very little well-resolved vibronic structure appears in the vicinity of this transition. The 136-cm^{-1} interval separating

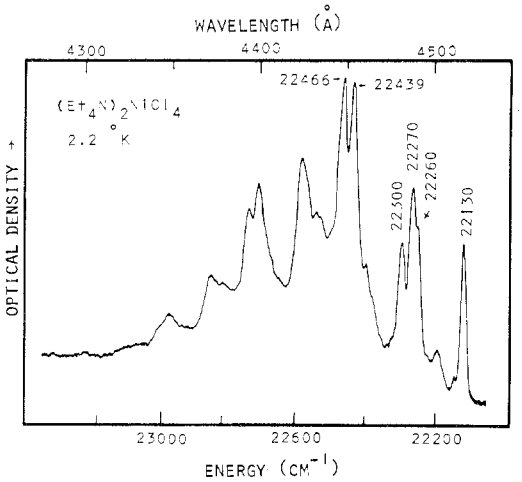

Figure 10. $^1E(^1G) \leftarrow {}^3T_1(^3F)$ transition in the single-crystal spectrum of $(Et_4N)_2NiCl_4$ at 2.2°K (4550–4300 Å).

the 19,620-cm^{-1} band from the origin suggests that it may be due to the $\nu_4(t_2)$ fundamental; however, it could be a vibronic origin based on the $A_2(\Gamma_4)$ component. The remaining bands are too diffuse to analyze in detail.

Since the broad band at 20,189 cm^{-1} is separated from the origin by 705 cm^{-1} and since it does not appear to be part of a progression (possibly based on the strong 19,620 cm^{-1} band), it is likely that it is vibronic structure based on the Γ_1 origin. The rather diffuse bands to higher energy can also be assigned in a similar fashion. This assignment is consistent with the emission spectrum (see Figure 11) which is analyzed assuming the Γ_1 state is located in this vicinity.

$^1E(^1G) \leftarrow {}^3T_1(^3F)$. Having no net electron spin, ^1E becomes Γ_3 and in D_{2d} the components are $A_1(\Gamma_3)$ and $B_1(\Gamma_3)$. Since pure electronic transitions to these states are forbidden, the structure appearing in Figure 10 must be solely due to vibronic origins. The b_2 and e components of the $\nu_3(t_2)$ and $\nu_4(t_2)$ fundamentals can give rise to a total of four vibronic origins, based on the $A_1(\Gamma_3)$ origin, and two vibronic origins can arise from the e components of these vibrations, based on the $B_1(\Gamma_3)$ origin. The spectrum can be analyzed completely if we assign the two bands at 22,130 and 22,300 cm^{-1} as vibronic origins based on the $B_1(\Gamma_3)$ state and the four bands at 22,260, 22,270, 22,439, and 22,466 cm^{-1} as vibronic origins based on the $A_1(\Gamma_3)$ state. If the 170-cm^{-1} separation between the $e(\nu_3)$ and $e(\nu_4)$ components in the $B_1(\Gamma_3)$ state is assumed to be the same in the $A_1(\Gamma_3)$ state, then the $A_1(\Gamma_3)$ state is determined to be 140 cm^{-1} to higher energy than the $B_1(\Gamma_3)$ state. Note that there is a progression in the 271-cm^{-1} totally symmetric $a_1(\nu_1)$ fundamental based on each of these origins. The detailed assignment of this spectrum appears in Table IV.

2. Emission Spectrum. The spectrum in Figure 11 is that of nickel in the $(Et_4N)_2ZnCl_4$ host. The two spectra were recorded photographically at different exposure times. In the lower tracing the four bands at 20,033, 20,018, 20,002, and 19,961 cm^{-1} serve as origins for a progression in an 825–835-cm^{-1} interval. The well-resolved bands at 19,100, 19,079, and 19,046 cm^{-1} also serve as similar origins. The appearance of these two band groups suggests that two different electronic transitions are responsible for the emission.

The assumption that these transitions arise from the same excited state leads to the following conclusions. If the pairs of bands at (20,018, 19,100 cm^{-1}), (20,002, 19,079 cm^{-1}) and (19,961, 19,046 cm^{-1}) correspond to one another in the two transitions, then the terminating electronic states are separated by 919 cm^{-1}. Since states arising from the $^3T_1(^3F)$ ground state are expected to have an overall energy spread of about 1100 cm^{-1},[16] it is likely that these states are the terminating states involved. Therefore the emitting level must be $^1A_1(^1G)$ or, equivalently, Γ_1 if it is assumed that it is at approximately the same energy in the doped compound as in the pure compound.

Table IV. Analysis of the $^1E(^1G) \leftarrow {}^3T_1(^3F)$ Transition in the Compound $(Et_4N)_2NiCl_4$[a]

Origin, cm^{-1}	Band energy, cm^{-1}	Energy diff, cm^{-1}	Assignment
Electronic: 22,012			$B_1(\Gamma_3)$
	22,130	118	$B_1(\Gamma_3) + e(\nu_4)$
	22,300	288	$B_1(\Gamma_3) + e(\nu_3)$
Vibronic: 22,130			^{ev}E
	22,201	71	$^{ev}E + a_1(\nu_2)$
	22,401	271	$^{ev}E + a_1(\nu_1)$
	22,674	544	$^{ev}E + 2a_1(\nu_1)$
Vibronic: 22,300			^{ev}E
	22,576	276	$^{ev}E + a_1(\nu_1)$
	22,851	551	$^{ev}E + 2a_1(\nu_1)$
Electronic: 22,152			$A_1(\Gamma_3)$
	22,260	108	$A_1(\Gamma_3) + b_2(\nu_4)$
	22,270	118	$A_1(\Gamma_3) + e(\nu_4)$
	22,439	287	$A_1(\Gamma_3) + e(\nu_3)$
	22,466	314	$A_1(\Gamma_3) + b_2(\nu_3)$
Vibronic: 22,260			$^{ev}B_2$
	22,534	274	$^{ev}B_2 + a_1(\nu_1)$
Vibronic: 22,270			^{ev}E
	22,543	273	$^{ev}E + a_1(\nu_1)$
	22,817	547	$^{ev}E + 2a_1(\nu_1)$
Vibronic: 22,439			^{ev}E
	22,709	270	$^{ev}E + a_1(\nu_1)$
	22,974	535	$^{ev}E + 2a_1(\nu_1)$
	23,243	804	$^{ev}E + 3a_1(\nu_1)$
Vibronic: 22,466			$^{ev}B_2$
	22,737	271	$^{ev}B + a_1(\nu_1)$
	23,012	546	$^{ev}B + 2a_1(\nu_1)$

[a] The associated spectrum appears in Figure 10.

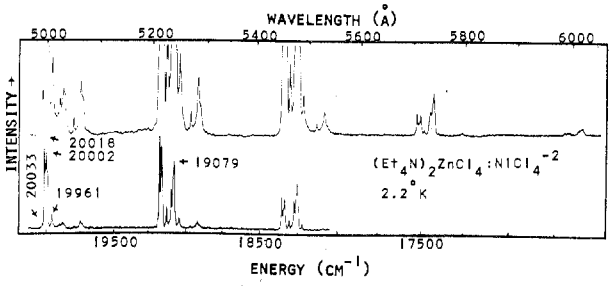

Figure 11. Emission spectrum of $(Et_4N)_2Zn(Ni)Cl_4$ at 2.2°K in the visible region (5000–6000 Å).

With spin–orbit coupling, the states Γ_1, Γ_3, Γ_4, and Γ_5 are derived from the $^3T_1(^3F)$ state. In T_d the transition from the Γ_1 state, derived from ^1G, is allowed to Γ_5. In D_{2d} the transition to the E component of the Γ_4 state becomes allowed. The LB calculation shows the Γ_4 and Γ_5 states as separated by about 800 cm^{-1}. Thus, the two band systems originating at 20,018 and 19,100 cm^{-1} can be assigned as transitions to Γ_4 and Γ_5, respectively.

The appearance of the highest energy transitions suggests that the 20,033-cm^{-1} band represents an origin upon which lattice vibrations are based, with an ~15-cm^{-1} frequency. The 72-cm^{-1} interval separating the 20,033-cm^{-1} origin and the 19,961-cm^{-1} band corresponds to the $\nu_2(e)$ fundamental. The 19,878-cm^{-1} band is assigned to the $\nu_4(t_2)$ fundamental, at a frequency of 140 cm^{-1}, and the 19,749-cm^{-1} band is assigned to either the $\nu_3(t_2)$ or $\nu_1(a_1)$ fundamental, with a frequency of 269 cm^{-1}. Similar assignments can be made for the $\Gamma_5 \leftarrow \Gamma_1$ system.

The very sharp features at 19,903 and 19,802 cm^{-1} (and the shoulder at 19,738 cm^{-1}) do not arise in any obvious way from tetrahedral fundamentals based on the 20,033-cm^{-1}

origin. Also transitions to the A_2 component of the Γ_4 state, the Γ_3 state, and the Γ_1 ground state are not observed.

Remaining to be explained is the nature of the 825–835-cm^{-1} interval. Since there are no tetrahedral $NiCl_4^{2-}$ (or $ZnCl_4^{2-}$) fundamentals at so high an energy, this interval must be due to a Et_4N^+ fundamental. Examination of the Raman and infrared spectra of the $(Et_4N)_2ZnCl_4$ compound shows a band at ~800 cm^{-1}. A vibration of this frequency can be assigned to the methyl–methylene–nitrogen, C–C–N, bending fundamental.[26] It would thus appear that this system of the tetrachloronickelate negative ion and tetraethylammonium cation is a unique example of an exciplex with a highly resolved emission spectrum.

Acknowledgment. We gratefully acknowledge the assistance of National Science Foundation Grant No. GP 16089 which financed this research.

Registry No. $(Et_4N)_2NiCl_4$, 5964-71-6; $(Et_4N)_2ZnCl_4$, 5964-74-9; Cs_3NiCl_5, 27976-95-0; Cs_3ZnCl_5, 20833-37-8.

References and Notes

(1) This work was completed as partial fulfillment of the requirements for the Ph.D. degree in chemistry at the University of Michigan.
(2) (a) C. R. Boston and G. Smith, *J. Phys. Chem.*, **62**, 409 (1958); (b) C. K. Jorgensen, *Mol. Phys.*, **1**, 410 (1958).
(3) D. M. Gruen and R. L. McBeth, *J. Phys. Chem.*, **63**, 393 (1959).
(4) N. S. Gill and R. S. Nyholm, *J. Chem. Soc.*, 3997 (1959).
(5) S. Buffagni and T. M. Dunn, *Nature (London)*, **188**, 937–938 (1960).
(6) C. Furlani and G. Monpurgo, *Z. Phys. Chem. (Frankfurt am Main)*, **28**, 93 (1961).
(7) D. M. L. Goodgame, M. Goodgame, and F. A. Cotton, *J. Am. Chem. Soc.*, **83**, 4161 (1961).
(8) R. Pappalardo, D. L. Wood, and R. C. Linares, *J. Chem. Phys.*, **35**, 1460 (1961).
(9) F. A. Cotton, O. D. Faut, and D. M. L. Goodgame, *J. Am. Chem. Soc.*, **83**, 344 (1961).
(10) R. Pappalardo and R. E. Dietz, *Phys. Rev.*, **123**, 1188 (1961).
(11) D. R. Stephens and H. G. Drickamer, *J. Chem. Phys.*, **35**, 429 (1961).
(12) H. A. Weakliem, *J. Chem. Phys.*, **36**, 2117 (1962).
(13) P. Day and C. K. Jorgensen, *J. Chem. Soc.*, 6226, (1964).
(14) B. D. Bird and P. Day, *J. Chem. Phys.*, **49**, 392 (1968).
(15) T. W. Couch and G. P. Smith, *J. Chem. Phys.*, **53**, 1336 (1970).
(16) A. D. Liehr and C. J. Ballhausen, *Ann. Phys. (N.Y.)*, **6**, 134 (1959).
(17) R. J. H. Clark and T. M. Dunn, *J. Chem. Soc.*, 1198 (1963).
(18) A. Sabatini and L. Sacconi, *J. Am. Chem. Soc.*, **86**, 17 (1964).
(19) Unpublished work.
(20) G. D. Stuckey, J. B. Folkers, and T. J. Kistenmacher, *Acta Crystallogr.*, **23**, 1064 (1967).
(21) J. Hanson, personal communication.
(22) R. P. van Stapele, H. G. Beljers, P. F. Bongers, and H. Zijlstra, *J. Chem. Phys.*, **44**, 3719 (1966).
(23) B. N. Figgis, M. Gerloch, and R. Mason, *Acta Crystallogr.*, **17**, 506 (1964).
(24) H. M. Powell and A. F. Wells, *J. Chem. Soc.*, 359 (1935).
(25) J. C. M. Henning and P. F. Bongers, *J. Phys. Chem. Solids*, **27**, 745 (1966).
(26) G. Herzberg, II, "Infrared and Raman Spectra of Polyatomic Molecules", Van Nostrand, Princeton, N.J., 1945.
(27) A. Mooney, R. H. Nuttall, and W. E. Smith, *J. Chem. Soc., Dalton Trans.*, 1096 (1972).
(28) A. Mooney, R. H. Nuttall, and W. E. Smith, *J. Chem. Soc., Dalton Trans.*, 1920 (1973).

Contribution from Ames Laboratory—USAEC and the Department of Chemistry, Iowa State University, Ames, Iowa 50010

Thermochemistry of Vanadium Oxytrichloride and Vanadium Oxytrifluoride by Mass Spectrometry

GERALD D. FLESCH and HARRY J. SVEC*

Received November 19, 1974 AIC40791S

Mass spectral and ionization efficiency data have been obtained for the positive and negative ions produced from $VOCl_3$ and VOF_3 by electron impact. From these data values have been calculated for several thermochemical parameters (eV): $IP_v(VOCl_3) = 11.90 \pm 0.05$, $IP_v(VOF_3) = 13.88 \pm 0.05$, $EA(VOCl_3) \geq 3.6$, $EA(VOF_3) = 3.1 \pm 0.3$, and $\Delta H_{f298}(VOF_3(g)) = -12.8 \pm 0.3$. Less precise values for these same parameters have been calculated for the observed positive and negative ion fragments and for the neutral fragments inferred to be produced in the mass spectrometer ion source. Bond energies (eV) are estimated to be $\bar{D}(V-O)_{VOCl_3} = 5.5$, $\bar{D}(V-Cl)_{VOCl_3} = 4.4$, $\bar{D}(V-O)_{VOF_3} = 5.9$, and $\bar{D}(V-F)_{VOF_3} = 5.8$. Bond energy values are also reported for the positive ion and neutral fragments.

Introduction

Several years ago there was considerable interest here in using volatile inorganic halides and oxyhalides as a means of introducing transition elements into a mass spectrometer for isotopic abundance studies.[1,2] These experiences provided some of the motivation for studies of the thermochemistry of these compounds. The paucity of mass spectral information about such compounds was also a factor. Baldock and Sites[3] briefly surveyed the mass spectra of $VOCl_3$ and VOF_3 in an investigation of possible feed materials for the electromagnetic separation of the vanadium isotopes. They made no detailed studies of the compounds. Svec[4] gave only preliminary results of studies of $VOCl_3$ and VOF_3 in a review of the mass spectrometry of volatile inorganic compounds. Ngai and Stafford[5] have reviewed the structure, thermochemistry, and mass spectra of various gaseous oxyhalides of transition elements and reported some data for $VOCl_3$ and VOF_3. In this report we present thermochemical information that can be obtained from a careful consideration of the ionization efficiency (IE) data generated when $VOCl_3$ and VOF_3 interact with energetic electrons. Singleton and Stafford[6] have reported correlations of mass spectra and ionization potentials which they observed in their studies of several oxyhalides of chromium, molybdenum, tungsten, rhenium, and osmium. Their work provides a test of some of the conclusions from the work now reported.

Experimental Section

The positive–negative ion mass spectrometer used in this research is a 6-in. 60°-sector instrument which has been described previously.[7] The instrument is operated with the ion source at ground potential and the two analyzer tubes at ±2200 V to extract and detect positive and negative ions simultaneously from a single electron beam.

All the mass spectral and IE data were accumulated using an ionizing current of 2 μA regulated at the anode. The mass spectral data were obtained with 70-V electrons and displayed on a strip chart recorder. The IE data were plotted by an X-Y recorder which is connected directly to the electron energy and ion current detectors.

The $VOCl_3$ and VOF_3 were prepared in the same manner as previously described for CrO_2Cl_2 and CrO_2F_2.[8] The vapors were admitted to the mass spectrometer at room temperature. The ion source temperature was estimated to be 65°.